Numerical Simulations of Wave Propagation: Time Reverse Imaging and Defect Mapping in Pipes

E. H. Saenger, C. Werner, L. T. Nguyen, G. K. Kocur, B. Ahrens

published in

NIC Symposium 2020
M. Müller, K. Binder, A. Trautmann (Editors)

Forschungszentrum Jülich GmbH,
John von Neumann Institute for Computing (NIC),
Schriften des Forschungszentrums Jülich, NIC Series, Vol. 50,
ISBN 978-3-95806-443-0, pp. 231.
http://hdl.handle.net/2128/24435

© 2020 by Forschungszentrum Jülich
Permission to make digital or hard copies of portions of this work for personal or classroom use is granted provided that the copies are not made or distributed for profit or commercial advantage and that copies bear this notice and the full citation on the first page. To copy otherwise requires prior specific permission by the publisher mentioned above.

Numerical Simulations of Wave Propagation: Time Reverse Imaging and Defect Mapping in Pipes

Erik H. Saenger[1,2], **Claudia Werner**[1,2], **Luan T. Nguyen**[1], **Georg K. Kocur**[3], **and Benedikt Ahrens**[1]

[1] International Geothermal Center Bochum, Lennershofstr. 140, 44801 Bochum, Germany
E-mail: {erik.saenger, claudia.werner, luan.nguyen, benedikt.ahrens}@hs-bochum.de

[2] Ruhr-University Bochum, Universitätsstr. 150, 44801 Bochum, Germany

[3] Institute of General Mechanics, RWTH Aachen University,
Templergraben 64, 52062 Aachen, Germany
E-mail: kocur@iam.rwth-aachen.de

Time reverse imaging (TRI) is evolving into a standard technique for locating and characterising seismic events. In recent years, TRI has been employed for a wide range of applications from the lab scale, to the field scale and up to the global scale. No identification of events or their onset times is necessary when locating events with TRI; therefore, it is especially suited for locating quasi-simultaneous events and events with a low signal-to-noise ratio. However, in contrast to more regularly applied localisation methods, the prerequisites for applying TRI are not sufficiently known. To investigate the significance of station distributions, complex velocity models and signal-to-noise ratios with respect to location accuracy, numerous simulations were performed using a finite difference code to propagate elastic waves through three-dimensional models.
Moreover, we present a reverse-time imaging technique by cross-correlating the forward wavefield with the reverse wavefield for the detection, localisation, and sizing of defects in pipelines. The presented technique allows to capture the wavefield reflectivity at the places of ultrasonic wave scattering and reflections. Thus, the method is suitable for detecting pipe defects of either point-like or finite-size types using data from a pulse-echo setup. By using synthetic data generated by 3D spectral element pipe models, we show that the 3D wavefield cross-correlation imaging is capable in the case of cylindrical guided ultrasonic waves. With a ring setup of transducers, we analyse the imaging results obtained from the synthetic single-transducer and all-transducer firings. The presented pipe flaw imaging method is straightforward to carry out using a suitable wave equation solver.

1 Time Reverse Imaging

The localisation and characterisation of seismic events in the subsurface are crucial for understanding physical processes in the Earth. Well-established methods are able to locate most seismic events in a fast and reliable manner; however, they rely on the identifiable onsets of events. Time reverse imaging (TRI) is a method especially suited for locating and characterising events which are indistinguishable in traces because they occur quasi-simultaneously and/or are superposed by noise. The prerequisites for more regularly applied localisation methods are very well known. However, the station distributions, the degree of complexity in the velocity model and the level of noise that hinder or enhance locating events with TRI are not sufficiently known. Therefore, this study systematically tests different station distributions for their localisation capabilities while considering complex velocity models and low signal-to-noise ratios. TRI uses the whole recorded waveform rendering the identification of events and their onsets obsolete. It can be applied as long as

the wave propagation can be described with a time-invariant wave equation. Seismic traces are reversed in time and back propagated through a medium until they focus on the initial event location. Imaging conditions are used to visualise aspects of the back-propagating wave field and obtain the source location. TRI has been applied in earth sciences as well as medical sciences for some time.[1] In recent years multiple studies have shown that TRI is a reliable, easy-to-use localisation tool: it has been used to retrieve source information on various scales from the lab scale in nondestructive testing,[2–5] over the field scale, for example in volcanic tremor[6] and non-volcanic tremor applications,[7, 8] and above hydrocarbon reservoirs,[9] up to the global scale.[10, 11] However, to apply TRI, a fairly accurate velocity model is needed to precisely back propagate the wave field. With the increasing availability of high resolution large three-dimensional velocity models and growing knowledge about prerequisites, TRI has the potential to locate seismic events, which could previously not be reliably located, over a wide range of applications.

1.1 Numerical Simulations for Time Reverse Imaging

The estimation of location accuracy is one major challenge when applying TRI. Therefore, a common approach is to perform a preliminary synthetic study to test if the given velocity model and station distribution enable reliable locations. If the synthetic study fails, the set-up is adjusted until either the study is abandoned or a sufficiently reliable result is achieved. This adjustment phase can be time-consuming because there are multiple characteristics appearing at once that may hinder the localisation.

A previous study by Werner and Saenger[12] aimed to find station distributions that produce reliable source locations with TRI. Finding these optimal station distributions is crucial to estimate the success rate of TRI with a given set of stations. In addition, the time needed to adjust station distributions may be decreased. Furthermore, the prerequisites of the method should be known when designing an array for TRI. Therefore, the influence of the station distribution, the complexity of the velocity model and the effect of different levels of noise on the location accuracy were investigated. Werner and Saenger[12] performed numerous simulations to systematically analyse different station distributions and their influence on the location accuracy of sources at different depths as well as analysing the influence of different source types. A typical example is shown in Fig. 1. Therefore, the focus was on the distance between receivers, the symmetry of the array in relation to the source position, the azimuthal gap between receivers and the number of stations. Simulations were first performed with a homogeneous velocity model and then with a complex velocity model. Location accuracy was investigated when the velocity model was known and when it was not specifically known. The authors[12] investigated the ability of TRI to cope with very low signal-to-noise ratios. The found guidelines using the methodical tests were applied to an actual real-life example in southern California. The ability to locate events at a target depth was investigated while using the existing array as well as the actual velocity model for a specific region in California.[13]

1.2 Discussion and Conclusion of Time Reverse Imaging

Werner and Saenger[12] showed that the inter-station distance should not be larger than the source depth, and that the aperture of the array should be at least twice the source depth.

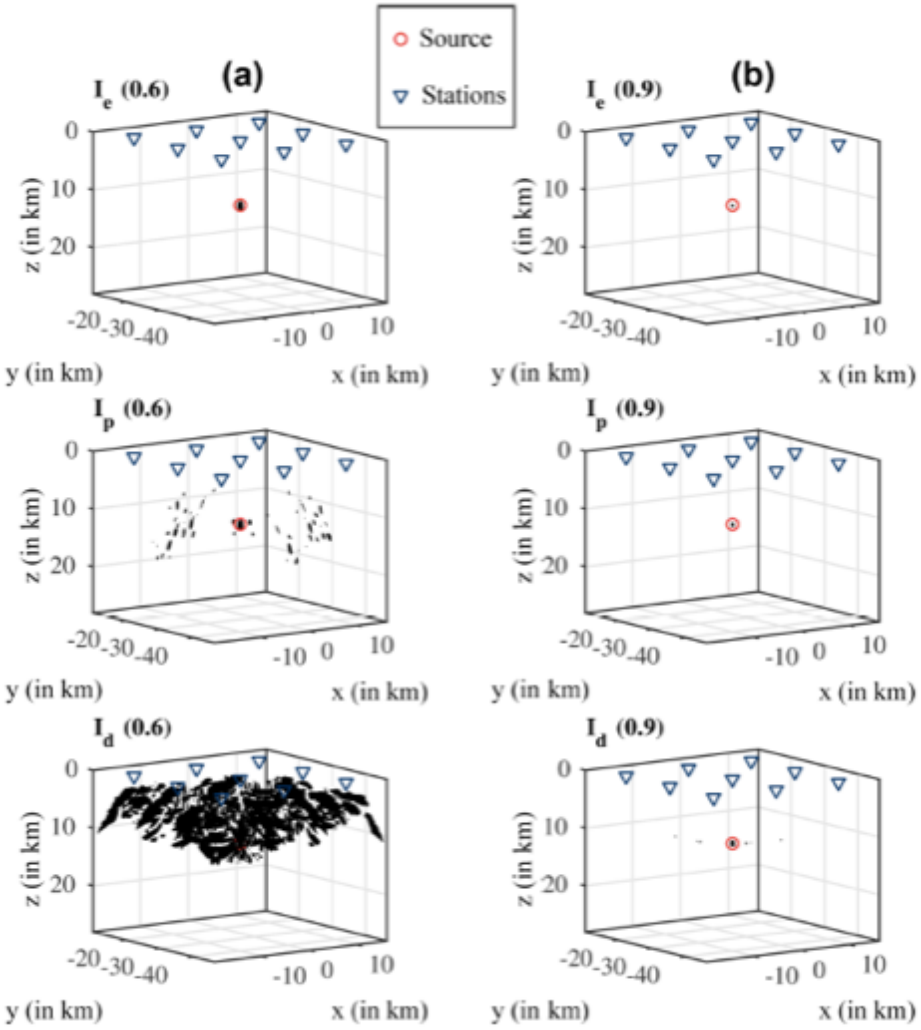

Figure 1. Imaging conditions plotted for one example simulation. Black spots are points with the values of 0.6 (in column a) and 0.9 (in column b) in the respective imaging conditions.[12]

Additionally, sources could be most accurately located when they were underneath the array. When using more stations, locations outside of the array became possible. In general, stations should be spaced regularly, although the deeper the source the more heterogeneously the stations can be and still achieve reliable locations. In addition to this strong sensitivity of the source location accuracy to the station distribution, the study found a strong influence of the velocity model on the localisation. However, complex velocity structures, like low velocity zones, do not hinder the localisation as long as they are adequately incorporated in the model. However, a high level of noise could inhibit the source

location even if the velocity model was homogeneous. An increased number of stations seemed to increase location accuracy in the presence of noise. Furthermore, an increase in location accuracy in some cases with an increase in complexity was observed, such as adding noise, more irregular stations or a more complex velocity model. This suggests that the additional scattering of waves may help the localisation. Therefore, the authors advise performing preliminary synthetic studies not only with homogeneous velocity models and regular stations but also incorporating as many complexities as possible to get an accurate estimation of the achievable source location. It was shown that only a few simulations are necessary when performing a preliminary synthetic study to estimate if the given set-up will work for TRI. Additionally, it was demonstrated that when designing an array to be used with TRI the target area should be considered. The depth of expected events then dictates the inter-station distance and the aperture of the array. If considering a range of depths, the inter-station distance should fit the shallowest events and the aperture of the deepest events.

2 Pipe Inspection

Guided ultrasonic waves are stress waves that propagate in a bounded solid medium. The use of ultra high frequency guided waves in nondestructive testing (NDT) of plate-like structures allows long-distance inspection capability, thus reducing the time and effort in collecting the ultrasound data and later in imaging possible defects. However, those guided waves propagate multi-modally and dispersively,[14] making interpretation of the ultrasound recordings complicated. Most often, ultrasonic excitations of the first few guided wave modes are used for ease of the ultrasound data analysis and interpretation.[15] If higher wave modes cannot be avoided (due to constraints of the inspected structures or transducers' bandwidths, and wave mode conversions), dispersion compensation and separation of propagation modes are sometimes needed.[16] Analytical, experimental, and numerical analyses of guided elastic waves in cylindrical rods and hollow cylinders[17] revealed complicated dispersive and multi-modal characteristics of cylindrical waves. Compared with Lamb waves in thin plate-like structures, cylindrical waves exhibit more complicated guided modes and dispersion characteristics (see Nguyen *et al.*[18] for more details). Flaw detection in pipework using guided waves has received great attention.[19] Most often, the degree of a defect is quantified based on a reflection coefficient expressed as a function of the geometrical extent of the defect.[20] To map defects in pipes, Leonard and Hinders[21] applied a type of travel time "cross-hole" tomography on the helical wave paths for building a tomographic flaw map of pipes. Gaul *et al.*[22] applied a synthetic focusing algorithm to the measured signals of the guided elastic waves in pipes. In another approach, Wang *et al.*[23] used a non-ring sparse sensor network of transducers to image pipe damage in an unwrapped grid based on the correlation of the first arrival waves. Also based on a sensor network of a non-ring configuration, Dehghan- Niri and Salamone[24] proposed to enhance damage-sensitive features, which are input to a reconstruction algorithm based on a waveform difference in baseline and measurement, by using multiple helical paths of the cylindrical waves. Hayashi[25] introduced a fast pipe thinning mapping method using amplitude spectrum peaks obtained from a laser based ultrasonic scanning system. Bagheri *et al.*[26] used the continuous wavelet and Hilbert transforms to extract damage-sensitive features and combined with a metaheuristic optimisation and a probabilistic approach to

construct an image of defects in pipe.

Time reversal in the manner of Fink[27] has also been found useful for NDT of thin-walled structures. By the time reversal principle, the recorded acoustic/elastic waveforms, if being time-reversed and reemitted at the receiving positions, form a wavefield that retraces its path back to the source location. When focused, the reverse wavefield becomes spatially concentrated and temporally compressed to reconstruct the original excitation pulse. Ing and Fink[28] experimentally showed that this time reversal invariance also holds for the dispersive Lamb waves. These features are important for the extrapolated reverse wavefield used in this work to be correctly back-propagated toward scattering and reflecting points. Other reports on structural health monitoring[29] showed that the time reversal principle can be applied to plates and composite structures for achieving baselinefree flaw detection even though dispersion does disturb refocusing of time reversed wave propagation. Xu and Giurgiutiu[29] and Park *et al.*[30] pointed out that time reversal creates sidebands around the true reconstructed impulse if more than one mode of the guided waves is excited. For pipe inspection, Hayashi and Murase[31] used the torsional T(0,1) mode for building a tomographic map of the pipe defects using the time reversal principle. Using the same cylindrical wave mode, Davies and Cawley[32] applied synthetic focusing based on time reversal operation in the frequency-wavenumber domain for pipe defect mapping. To the best of the authors' knowledge, in NDT applications for both plates and pipes, however, the time reversal principle is mostly limited to the location of point-like acoustic sources and scatterers and the reconstruction of the source wavelets. Nguyen *et al.*[18] introduced the use of the wavefield cross-correlation method for flaw detection and sizing in waveguides with a particular application for the inspection of pipework. It was shown that the so-called reverse-time migration, which is based on a zero-lag cross-correlation between the forward wavefield and the reverse wavefield, can be efficiently used for detecting, locating, and sizing flaws of abrupt material changes such as cracks, eroded/corroded voids, and local material damages caused by, for example, impacts in pipes. As this is a method for imaging of reflectors, it can be used to detect and locate both point-like scatterers and finite-size defects.

2.1 Guided Wave Propagation in Pipes

The motions of elastic wave propagation in a pipe, as for other thin-walled structures, are guided within the pipe wall. However, unlike in plates, there exist three distinct families of wave modes in pipes: the axisymmetric longitudinal modes L(0,m), the non-axisymmetric flexural modes F(n,m), and the torsional modes T(0,m) (where m and n are the radial and circumferential mode parameters, respectively[33]). The longitudinal wave modes L(0,1) and L(0,2) correspond to the fundamental anti-symmetric A0 and symmetric S0 Lamb modes, respectively. The torsional mode T(0,1) is equivalent to SH waves in a plate. Detailed solutions of the elastic wave problem in hollow and solid cylinders are studied in Ref. 17 and their modal relation to those in plates are discussed in Ref. 34. Generally, the results show, for the same ratio of thickness-to-diameter, the dispersion characteristics of the axisymmetric longitudinal modes in cylindrical waves are comparable to those of Lamb waves in a plate at the high-frequency range. The similar behaviour is observed if the thickness-to-diameter ratio decreases. The significant difference in the dispersion characteristics between the cylindrical modes and Lamb modes lies in the low-frequency

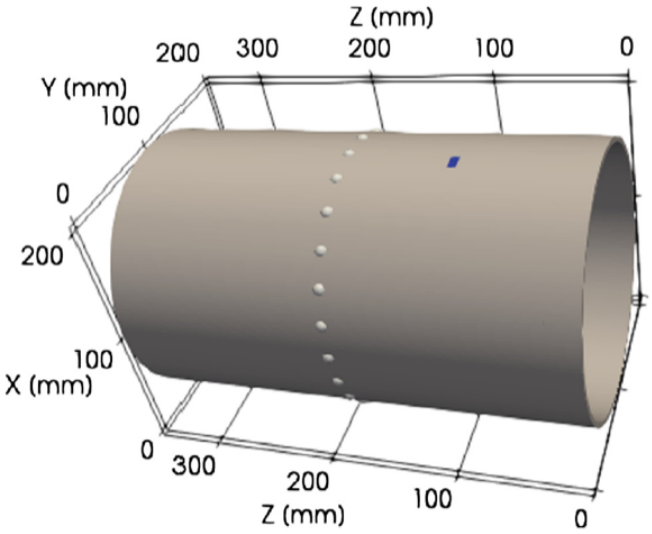

Figure 2. 3D model of a 350 mm long portion of a straight steel pipe with a through-thickness rectangular defect (the blue coloured area).[18] The dots around the pipe circumference represent the positions of the ultrasound transducers arranged at 15 degree intervals.

range. For example, as the frequencies decrease, the phase velocity of the L(0,1) mode of cylindrical waves approaches the S0 Lamb mode instead of approaching zero propagating velocity as for the A0 Lamb mode.

Nguyen *et al.*[18] examined wave propagation in a 350 mm long steel pipe having a small-size through-thickness voided defect as shown in Fig. 2. Because the imaging method requires access to the full ultrasonic wavefields, an efficient 3D elastic wave solver that can handle complex geometries is desirable. 3D guided elastic wavefields were simulated for the pipe model using SPECFEM3D.[35] In addition to an efficient forward solver, SPECFEM3D also provides reversetime simulation and adjoint capabilities instrumental for waveform tomography and imaging. The discretised model consists of 92160 hexahedral elements and is simulated with time stepping of 35 ns. All boundaries including the pipe ends are modelled as traction-free. Based on the dispersion characteristics of guided waves, it is considered advantageous to select a source time function that is narrowband to reduce the number of the excited wave modes and dispersive behaviour during wave propagation. However, a narrowband excitation also means long-duration propagating wave packets in the time domain, which may cause a loss of focus of the reverse wavefield in the imaging. Here, the study examined the effects of narrowband Hanning windowed toneburst and the broadband Ricker wavelet as input signals, both centred at 200 kHz. The choice of the central frequency depends on the imaging resolution one wants to resolve taken into consideration that a higher frequency may excite higher order guided wave modes. Although not formally studied in this work, central frequency around 200 kHz appears to be satisfactory for imaging the simulated defects.

2.2 Wavefield Cross-Correlation Imaging

In reverse-time imaging, the used imaging condition governs the reconstruction capability of an imaging method. To reconstruct a reflectivity image of possibly multiple reflecting and scattering defects in a pipe, the forward wavefield was cross-correlated with the reverse wavefield, which is the working principle behind reverse-time migration (RTM).[36] This imaging condition is based on the princle that wave reflection and scattering happen at places where the source wavefield is time coincient with the receiver re-emited wavefield. Hence, this imaging technique differs greatly from a type of Kirchhoff migration, which is based on the ray assumption of propagating waves, commonly used in ultrasound NDT within implementations of the delay-and-sum synthetic aperture focusing technique (SAFT).[37] RTM, as based on simulating the full wave equation of a possibly heterogeneous velocity model, can be superior to SAFT in delivering higher resolution and more accurate imaging results. RTM also differentiates itself from the popular time reversal multiple signal classification (MUSIC), which calculates scattering intensity at the image points based on the inner products of the Green's function and the noise vectors obtained from singular value decomposition of the time reversal operator.[38]

In ultrasound NDT, RTM of the body waves has recently been used for locating damaged features, hidden interfaces, and boundaries of the civil engineering structures.[39, 40] Concerning NDT of plate-like structures, a small number of published articles reported on the use of RTM for NDT of laminated composite plates within implementations of the excitation-time imaging condition[41] and the zero-lag wavefield cross-correlation imaging condition.[42] The imaging condition by RTM in this work is based on the zero-lag wavefield cross-correlation.[36] So, the final reflectivity image is obtained by performing an entrywise product in space of the forward (source) wavefield and the reverse (receiver) wavefield and cross-correlating them in time following an imaging algorithm (more details are presented in the Appendix A of Nguyen *et al.*[43]). The cross-correlated image adds up constructively at time when the reverse wavefield is spatially refocused and at place where wave scattering and reflection take place.

The homogeneous intact pipe model is used to simulate the forward and reverse wavefields required in the imaging step. Fig. 3 illustrates the stepwise reverse-time imaging process at three selected timesteps: Before focusing, at focusing, and long after focusing of the reverse wavefield takes place. The cross-correlation results in Fig. 3 show that the spatial reconstruction of the defect is captured at the time the forward wavefield and the re-focused reverse wavefield coincide (the second selected timestep in Fig. 3b). After the refocusing of the reverse wavefield, the cross-correlated reconstruction remains relatively unchanged (Fig. 3c). Although the wavefields and the resulting cross-correlated image are three-dimensional, only the fields at the outer surface of the pipe are displayed in Fig. 3. The reconstructed images are normalised to their reflectivity range. This style of plotting applies to the rest of wavefield plots and reflectivity images.

2.3 Discussion and Conclusion of Wavefield Cross-Correlation Imaging

Nguyen *et al.*[18] have presented the wavefield cross-correlation whose imaging principle is sound and its implementation is straightforward.[18] The cross-correlation of the simulated full 3D ultrasonic wavefields honours the kinematics of the wave phenomena. The synthetic verification of this imaging technique for defect mapping in pipes demonstrates

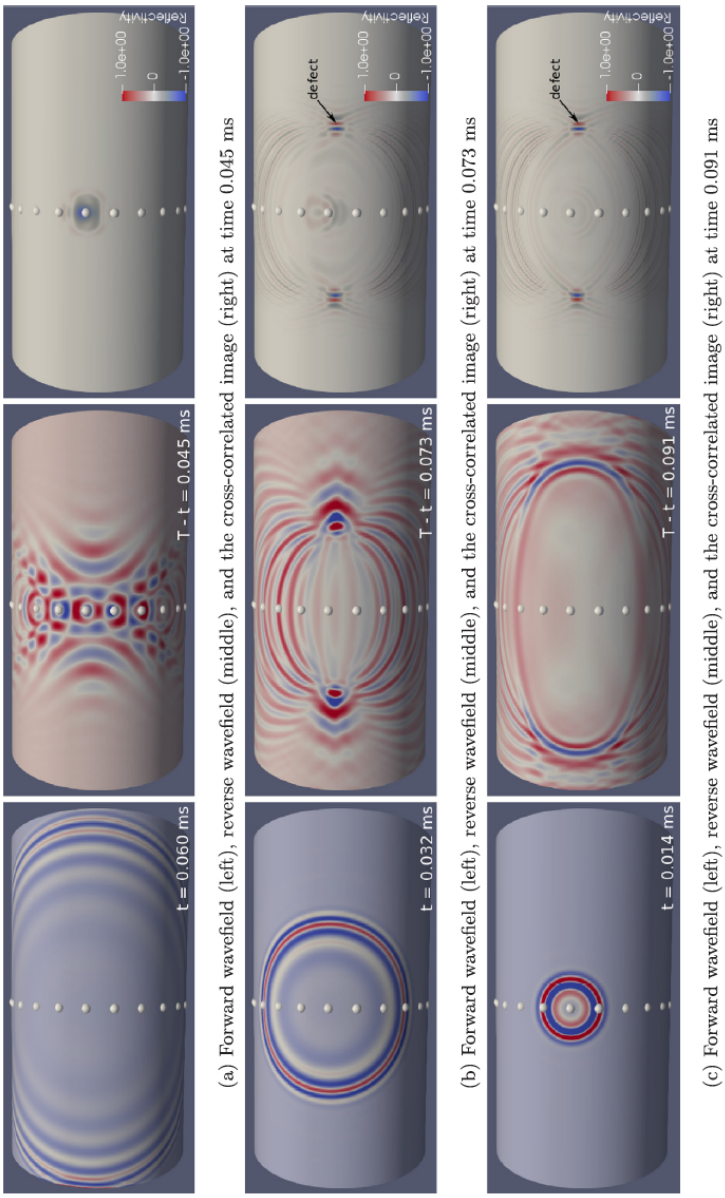

Figure 3. Wavefield snapshots of the cross-correlation imaging process at three selected time steps: (a) before focusing, (b) at focusing, and (c) after focusing of the reverse wavefield has passed.[18] Left column: the forward wavefield is accessed backward in time in the order (a) 0.06 ms, (b) 0.032 ms, and (c) 0.014 ms. Middle colum: the reverse wavefield is accessed forward in time in the order (a) 0.045 ms, (b) 0.073 ms, and (c). 0.091 ms. In the forward and reverse wavefields, displacement field in x-direction is plotted.

its ability to reconstruct a quality image of possibly multiple flaws. Unlike solving an inverse problem, this wave-equation based imaging does not suffer from running long iterations and the risk of arriving at an unfaithful reconstruction (local-minimum solution). For engineered structures undergone non-destructive testing, such as the pipe, the wave velocity and density maps are often homogeneous and known, giving very good conditions for applying the presented imaging method. Concerning computational effort, using the supershot setup[18] greatly expedites the imaging procedure compared with using a number of single element shots. Imaging using no baseline data is also more easily performed on data resulting from the supershot setup and has been demonstrated in this work.

The reverse-time imaging by cross-correlating the forward and reverse wavefields of the guided waves is shown to be highly efficient in constructing a sharply focused reflectivity image of the defects in pipes. The presented implementation is advantageous in that it involves no algorithmic parameters to tune. If post-processing, such as smoothing, of the reconstructed image is required to emphasise specific defected features, the involved image processing can be quickly done given a few input parameters of the filtering kernel. This imaging procedure can be applied and extended to nondestructive evaluation of pipes of arbitrary geometries such as bend pipes or pipes of multiple layers and varying thicknesses and other 3D waveguide structures even in the case of wave interactions with the surrounding environment such as soil and water are present.

Acknowledgements

The authors gratefully acknowledge the computing time granted by the John von Neumann Institute for Computing (NIC) and provided on the JURECA supercomputer at the Jülich Supercomputing Centre (JSC), Germany.

References

1. M. Fink, D. Cassereau, A. Derode, C. Prada, P. Roux, M. Tanter, J.-L.Thomas, and F. Wu, *Time-reversed acoustics*, Reports Prog. Phys. **281**, 91–97, 1999.
2. E. H. Saenger, *Time reverse characterization of sources in heterogeneous media*, NDT E. Int. **44**, 751–759, 2011.
3. B. E. Anderson, M. Griffa, T. J. Ulrich, and P. A. Johnson, *Time reversal reconstruction of finite sized sources in elastic media*, J. Acoust. Soc. Am. **130**, EL219–EL225, 2011.
4. B. M. Harker and B. E. Anderson, *Optimization of the array mirror for time reversal techniques used in a halfspace environment*, J. Acoust. Soc. Am. **133**, EL351–EL357, 2013.
5. G. K. Kocur, E. H. Saenger, C. U. Grosse, and T. Vogel, *Time reverse modeling of acoustic emissions in a reinforced concrete beam*, Ultrasonics **65**, 96–104, 2016.
6. I. Lokmer, G. S. O'Brien, D. Stich, and C. J. Bean, *Time reversal imaging of synthetic volcanic tremor sources*, Geophys. Res. Lett. **36**, 1–6, 2009.
7. C. S. Larmat, R. A. Guyer, and P. A. Johnson, *Tremor source location using time reversal: Selecting the appropriate imaging field*, Geophys. Res. Lett. **36**, 2–7, 2009.

8. T. Horstmann, R. M. Harrington, and E. S. Cochran, *Using a modified time-reverse imaging technique to locate low-frequency earthquakes on the San Andreas Fault near Cholame, California*, Geophys. J. Int. **203**, 1207–1226, 2015.
9. B. Steiner, E. H. Saenger, and S. M. Schmalholz, *Time reverse modeling of low-frequency microtremors: Application to hydrocarbon reservoir localization*, Geophys. Res. Lett. **35**, L03307, 2008.
10. C. S. Larmat, J. P. Montagner, M. Fink, Y. Capdeville, A. Tourin, and E. Clévédé, *Time-reversal imaging of seismic sources and application to the great Sumatra earthquake*, Geophys. Res. Lett. **33**, L19312, 2006.
11. C. S. Larmat, J. Tromp, Q. Liu, and J. P Montagner, *Time reversal location of glacial earthquakes*, J. Geophys. Res.-Solid **113**, 1–9, 2008.
12. C. Werner and E. H. Saenger, *Obtaining reliable source locations with time reverse imaging: limits to array design, velocity models and signal-to-noise ratios*, Solid Earth **9**, 1487–1505, 2018.
13. X. Zeng, C. H. Thurber, D. R. Shelly, R. M. Harrington, E. S. Cochran, N. L. Bennington, D. Peterson, B. Guo, and K. McClement, *3-D P- and S-wave velocity structure and low-frequency earthquake locations in the Parkfield, California region*, Geophys. J. Int. **206**, 1574–1585, 2016.
14. H. Lamb, *On waves in an elastic plate, Proceedings of the Royal Society of London A: Mathematical*, Physical and Engineering Sciences **93**, 114–128, 1917.
15. D. N. Alleyne and P. Cawley, *Optimization of Lamb wave inspection techniques*, NDT E Int. **25**, 11–22, 1992.
16. P. D. Wilcox, *A rapid signal processing technique to remove the effect of dispersion from guided wave signals*, IEEE Trans. Ultrason. Ferroelectr. Freq. Control **50**, 419–427, 2003.
17. J. Zemanek Jr., *An experimental and theoretical investigation of elastic wave propagation in a cylinder*, J. Acoust. Soc. Am. **51**, 265–283, 1972.
18. L. T. Nguyen, G. K. Kocur, and E. H. Saenger, *Defect mapping in pipes by ultrasonic wavefield cross-correlation*, Ultrasonics **90**, 153–165, 2018.
19. J. Zemanek, *Defect detection in pipes using guided waves*, Ultrasonics **36**, 147–154, 1998.
20. B. Vogelaar and M. Golombok, *Quantification and localization of internal pipe damage*, Mech. Syst. Signal Process. **78**, 107–117, 2016.
21. K. R. Leonard and M. K. Hinders, *Guided wave helical ultrasonic tomography of pipes*, J. Acoust. Soc. Am. **114**, 767–774, 2003.
22. T. Gaul, L. Schubert, B. Weihnacht, and B. Frankenstein, *Localization of defects in pipes using guided waves and synthetic aperture focussing technique (SAFT)*, in EWSHM-7th European Workshop on Structural Health Monitoring, 2014.
23. Q. Wang, M. Hong, and Z. Su, *A sparse sensor network topologized for cylindrical wave- based identification of damage in pipeline structures*, Smart Mater. Struct. **25**, 075015, 2014.
24. E. Dehghan-Niri and S. Salamone, *A multi-helical ultrasonic imaging approach for the structural health monitoring of cylindrical structures*, Struct. Health Monit. **14**, 73–85, 2015.
25. T. Hayashi, *Non-contact imaging of pipe thinning using elastic guided waves generated and detected by lasers*, Int. J. Press. Vessels Pip. **153**, 26–31, 2017.

26. A. Bagheri, P. Rizzo, and K. Li, *Ultrasonic imaging algorithm for the health monitoring of pipes*, J. Civil Struct. Health Monit. **7**, 99–121, 2017.
27. M. Fink, *Time reversal of ultrasonic fields. I. Basic principles*, IEEE Trans. Ultrason. Ferroelectr. Freq. Control **39**, 555–566, 1992.
28. R. K. Ing and M. Fink, *Time-reversed Lamb waves*, IEEE Trans. Ultrason. Ferroelectr. Freq. Control **45**, 1032–1043, 1998.
29. B. Xu and V. Giurgiutiu, *Single mode tuning effects on Lamb wave time reversal with piezoelectric wafer active sensors for structural health monitoring*, J. Nondestr. Eval. **26**, 123–134, 2007.
30. H. W. Park, S. B. Kim, and H. Sohn, *Understanding a time reversal process in Lamb wave propagation*, Wave Motion **46**, 451–467, 2009.
31. T. Hayashi and M. Murase, *Defect imaging with guided waves in a pipe*, J. Acoust. Soc. Am. **117**, 2134–2140, 2005.
32. J. Davies and P. Cawley, *The application of synthetic focusing for imaging crack-like defects in pipelines using guided waves*, IEEE Trans. Ultrason. Ferroelectr. Freq. Control **56**, 759–771, 2009.
33. H. Nishino, S. Takashina, F. Uchida, M. Takemoto, and K. Ono, *Modal analysis of hollow cylindrical guided waves and applications*, Jpn. J. Appl. Phys. **40**, 364, 2001.
34. A. Velichko and P. D. Wilcox, *Excitation and scattering of guided waves: Relationships between solutions for plates and pipes*, J. Acoust. Soc. Am. **125**, 3623–3631, 2009.
35. D. Komatitsch and J. Tromp, *Introduction to the spectral element method for three-dimensional seismic wave propagation*, Geophys. J. Int. **139**, 806–822, 1999.
36. J. F. Claerbout, *Toward a unified theory of reflector mapping*, Geophysics **36**, 467–481, 1971.
37. M. Schickert, M. Krause, and W. Müller, *Ultrasonic imaging of concrete elements using reconstruction by synthetic aperture focusing technique*, J. Mater. Civil Eng. **15**, 235–246, 2003.
38. F. K. Gruber, E. A. Marengo, and A. J. Devaney, *Time-reversal imaging with multiple signal classification considering multiple scattering between the targets*, J. Acoust. Soc. Am. **115**, 3042–3047, 2004.
39. M. Grohmann, S. Müller, E. Niederleithinger, and S. Sieber, *Reverse time migration: introducing a new imaging technique for ultrasonic measurements in civil engineering*, Near Surface Geophys. **15**, 242–258, 2017.
40. L. T. Nguyen and R. T. Modrak, *Ultrasonic wavefield inversion and migration in complex heterogeneous structures: 2D numerical imaging and nondestructive testing experiments*, Ultrasonics **82**, 357–370, 2018.
41. L. Wang and F. G. Yuan, *Damage identification in a composite plate using prestack reverse-time migration technique*, Struct. Health Monit. **4**, 195–211, 2005.
42. J. He and F.-G. Yuan, *Damage identification for composite structures using a cross-correlation reverse-time migration technique*, Struct. Health Monit. **14**, 558–570, 2015.
43. L. T. Nguyen, G. K. Kocur, and E. H. Saenger, *Defect mapping in pipes by ultrasonic wavefield cross-correlation: A synthetic verification*, Ultrasonics **90**, 153–165, 2018.